PERGAMON

Journal of Structural Geology 22 (2000) 1325–1339

JOURNAL OF STRUCTURAL GEOLOGY

www.elsevier.nl/locate/jstrugeo

Ultramylonite bands derived from cataclasite and pseudotachylyte in granites, northeast Japan

Hideo Takagi*, Kiyohiko Goto [1], Norio Shigematsu

Department of Earth Sciences, School of Education, Waseda University, Shinjuku, Tokyo 169-8050, Japan

Received 20 July 1998; accepted 20 March 2000

Abstract

Small-scale ultramylonite and cataclasite bands, millimeters to tens of centimeters thick, are developed in granitic rocks west of the Hatagawa Fault Zone (HFZ) in the Abukuma Belt, northeast Japan. They occur as single or paired bands with sharp planar boundaries trending NNE–SSW, and often form networks and conjugate sets. The very small *S–C* angle and the high displacement/thickness ratio of the bands suggest that the shear strain is high. The ultramylonite bands are commonly associated with cataclasite bands and mineral veins, and rarely with pseudotachylyte. Some cataclasite bands contain mylonitized layers in which quartz fragments are strongly deformed and dynamically recrystallized. On the other hand, some ultramylonites are fractured producing fragments that have rotated during later cataclasis.

The major element content of the ultramylonite bands is similar to that of the surrounding granitic rocks, strongly suggesting that the ultramylonite bands have formed through in-situ deformation of the granitic protolith without significant mass transfer. Mineralogy and microstructures of some ultramylonites suggest the strong possibility that they are derived from pseudotachylyte. The ultramylonite bands are interpreted as forming in the 10–15-km-deep cataclastic–plastic transition zone under greenschist facies conditions where co-seismic fracturing and aseismic plastic flow have alternated.

1. Introduction

Earthquakes along intracontinental fault zones commonly occur in the shallow part of the continental crust (2–18 km), representing the seismogenic zone (Sibson, 1982, 1983; Scholz, 1988), and the focal depth of large earthquakes lies at the base of the zone (Sibson, 1982; Das and Scholz, 1983). For example, the focal depth of the main shock of the Loma Prieta earthquake in California (M7.1) in 1989 was about 18 km, whereas the focal depths of the aftershocks varied from 2 to 19 km (U.S. Geological Survey Staff, 1990). The focal depth of the main shock of the Hyogoken-nanbu earthquake in Kobe (M7.2) in 1995 was about 17 km, whereas the focal depths of the aftershocks varied from 3 to 15 km (Ando, 1995).

The rheological properties of the rocks in the continental crust are expected to change from brittle fracturing and cataclastic flow (cataclastic domain) at shallow depths to dominantly plastic flow (plastic domain) at deeper levels. It has been recognized that the restriction of the seismogenic zone to shallow depths of the continental crust reflects this difference in rheological properties (Sibson, 1977; Scholz, 1990). Byerlee (1978) demonstrated that the shear strength of rocks increases almost linearly with confining pressure in the cataclastic domain due to the operation of a Coulomb frictional law. On the other hand, shear strength decreases as ambient temperature increases in the plastic domain according to most creep laws (e.g. Hobbs et al., 1976). Accordingly, the shear strength must be a maximum at the cataclastic–plastic transition zone (Brace and Kohlstedt, 1980; Kirby, 1980),

* Corresponding author.
E-mail address: hideo@mn.waseda.ac.jp (H. Takagi).
[1] Present address: JR Tokai Construction Co., Ltd, Nakamura-ku, Nagoya 453-0014, Japan.

0191-8141/00/$ - see front matter
PII: S0191-8141(00)00034-1

and thus the elastic strain energy is also a maximum here. Small earthquakes occurring at shallow depth cannot propagate deeper into the higher strength region, and thus they cannot rupture the whole fault surface. This is considered as the main reason why large earthquakes almost invariably nucleate near the base of the seismogenic zone (Das and Scholz, 1983).

The close association of cataclastically and plastically formed fault rocks is expected at the base of the seismogenic zone. Fault gouges and cataclasites are common products of rock fracturing in the cataclastic domain, whereas mylonites are common products associated with plastic flow of fine-grained mineral aggregates constituting matrix (e.g. Sibson, 1977; Passchier and Trouw, 1996) in the plastic domain. Pseudotachylyte is commonly associated with cataclasite in the cataclastic domain. However, based on the close association of pseudotachylyte and cataclasite with mylonite, it has been suggested that this assemblage formed in the cataclastic–plastic transition zone (Sibson, 1980; Passchier, 1982, 1984; Hobbs et al., 1986; Koch and Masch, 1992; White, 1996; Tourigny and Tremblay, 1997; Guermani and Pennacchioioni, 1998; Takagi, 1998). Detailed analysis of this cataclastic–plastic fault rock association, therefore, should provide a better understanding of the rheological processes responsible for intracontinental large earthquakes which have a fairly deep focal depth (20–15 km).

Thinly developed (millimeters to tens of centimeters thick) shear zones, including dark and flinty fault rocks (dark bands), are developed on the west of the Hatagawa Fault Zone (HFZ) in the Abukuma Mountains, northeast Japan (Goto et al., 1994; Shigematsu and Goto, 1995). Goto et al. (1994) referred to these foliated and lineated dark shear zones as ultramylonite bands. Some of the dark bands are also composed of cataclasite (Shigematsu and Goto, 1995), mylonitized cataclasite (Takagi, 1998), and foliated pseudotachylyte (Kubo and Takagi, 1997). This paper presents data on meso- and microstructures and bulk chemical composition of the dark bands and compares them to those of granitic protolith along the HFZ. The possibility that they are formed in the cataclastic–plastic transition zone is discussed, as is the time–space relationship between the seismogenic fracturing and plastic flow.

2. Geologic outline

Mid-Cretaceous granitoids are widely distributed in the Abukuma Mountains in northeast Japan. Two major fault zones trending NNW–SSE, the HFZ on the west and the Futaba Fault Zone on the east, are developed in the eastern margin of the Abukuma Mountains. The HFZ forms the boundary between the Abukuma Belt on the west and the South Kitakami Belt on the east (Kubo and Yamamoto, 1990; Kubo et al., 1990, 1994). Both belts in the study area are mainly composed of granitic rocks.

In the study area around the Takase River near Namie town (Fig. 1), the granitic rocks on the west of the HFZ are classified as hornblende-bearing biotite granodiorite and pink biotite granite. The K–Ar ages for the granitic rocks are about 95–100 Ma (Kubo and Yamamoto, 1990). A cataclasite zone with a thickness of a few tens of meters trends N15°W. The western geologic boundary of this zone is considered to be the main fault of the HFZ, the type locality of which is along the Takase River, west of Hatagawa (Fig. 1). The fault surface strikes N5°W and dips 86°W, and is associated with a dark greenish gray fault gouge zone (ca. 60 cm thick) with a dark brecciated zone 11 m thick on the east. The slickenline on the fault surface is nearly horizontal or plunging at 10°N. Greenstones, greenish pelites and psammites, and limestones are tectonically intercalated as small lenticular bodies in the granitic rocks on the west of the main fault. These rocks are correlative with the Paleozoic strata of the South Kitakami Belt.

Fault rocks on the east of the HFZ in the South Kitakami Belt are characterized by a sinistral ductile shear zone (mylonite zone) with a thickness of 1–3 km in the study area (Koshiya, 1988; Shigematsu, 1994). This ductile shear zone trends N–S oblique to the main fault (N15°W). Shear strain decreases eastward from the main fault (Fig. 1, Shigematsu, 1994). The age of sinistral ductile shearing along this shear zone is estimated to be 106–86 Ma (Otsuki and Ehiro, 1992).

Small-scale shear zones millimeters to several tens of centimeters in thickness are sporadically developed in the non-deformed Abukuma granites about 1–3 km west from the main fault of the HFZ. The region containing these dark bands extends along 25 km from north to south with 1–2 km width in the Ukedo River and the Takase River areas (Fig. 2). These small-scale shear zones commonly contain dark, flinty and very fine-grained bands (dark bands).

3. Mesoscopic structures

The foliation of the dark bands subparallel to their margins strikes mainly NNE and partly E–W, and generally dips steeply (Fig. 2a). On the surface of dark bands, a ridge-in-groove and/or stretching mineral lineation is commonly observed. The dominant orientation has a plunge of 40° NNE, although a subsidiary trend is N–S with a gentle southerly plunge (Fig. 2b)

Typical occurrence of the dark bands in an outcrop along the Takase River is shown in Fig. 3 (A in Fig. 1).

Some dark bands contact sharply with undeformed massive granite (Fig. 4a–c), whereas other dark bands contact transition zones composed of protomylonite–mylonite in which sigmoidally shaped foliations are observed (Fig. 4d–f). Some dark bands are parallel to veins of aplite, quartz and epidote. The thickness of the dark bands varies from several millimeters to several tens of centimeters. Some dark bands are continuous with fractures past their termination. Dark bands are generally single and straight (Fig. 4a, e), but some

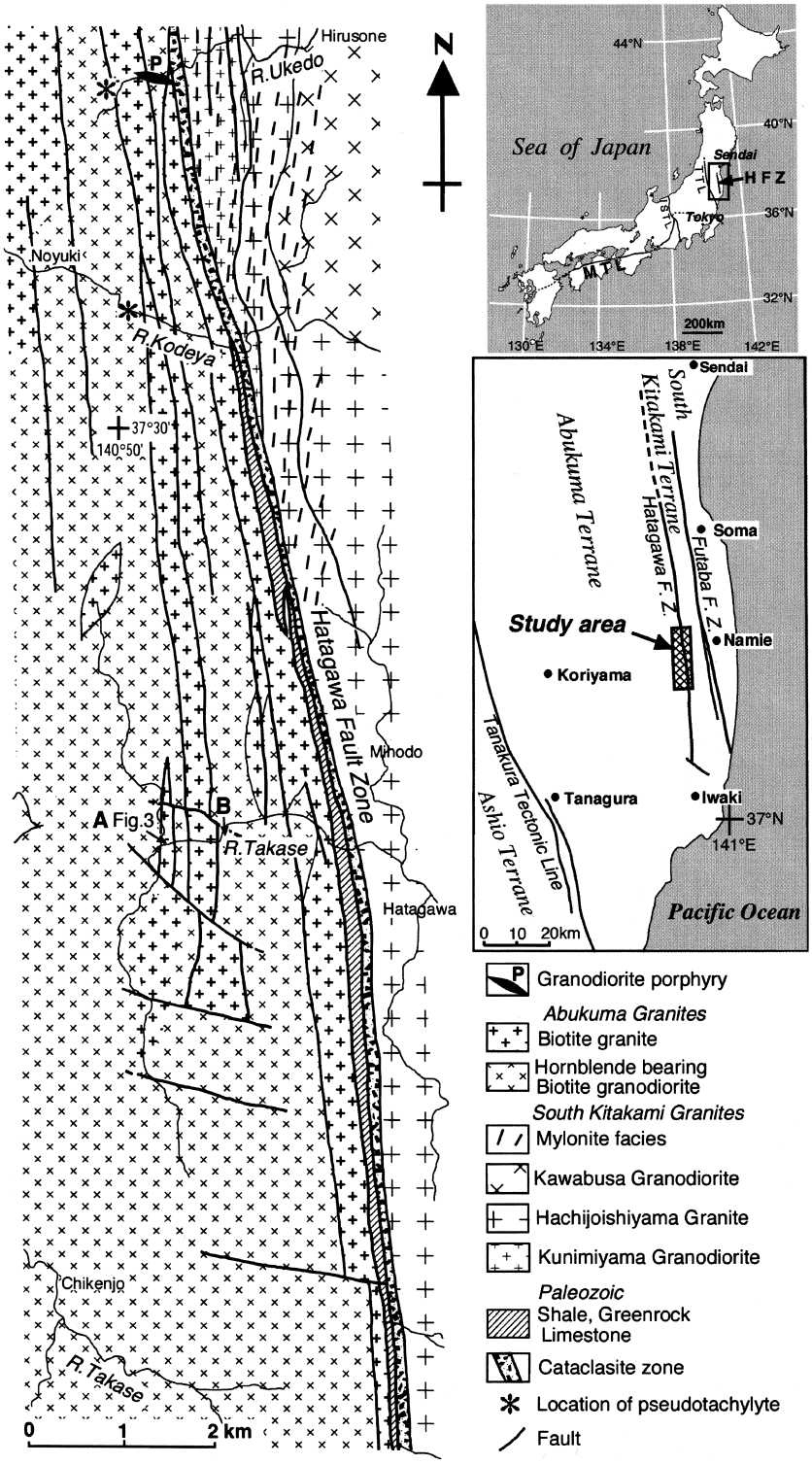

Fig. 1. Geologic map with index maps of the Abukuma and South Kitakami belts along the Hatagawa Fault Zone, NE Japan.

of them branch out (Fig. 4b, d), or form paired parallel shear zones (Fig. 4f). Some of the dark bands form conjugate sets, and others have a network pattern (Fig. 4c).

Well-foliated dark bands have thin (ca. 2 mm) layering (Fig. 4a, e, f), subparallel to the band boundary. The angle between the foliation and band boundary is generally very small (e.g. Fig. 4f), indicating finite shear strain (γ) is very large.

Fig. 5 shows the relationship between the thickness

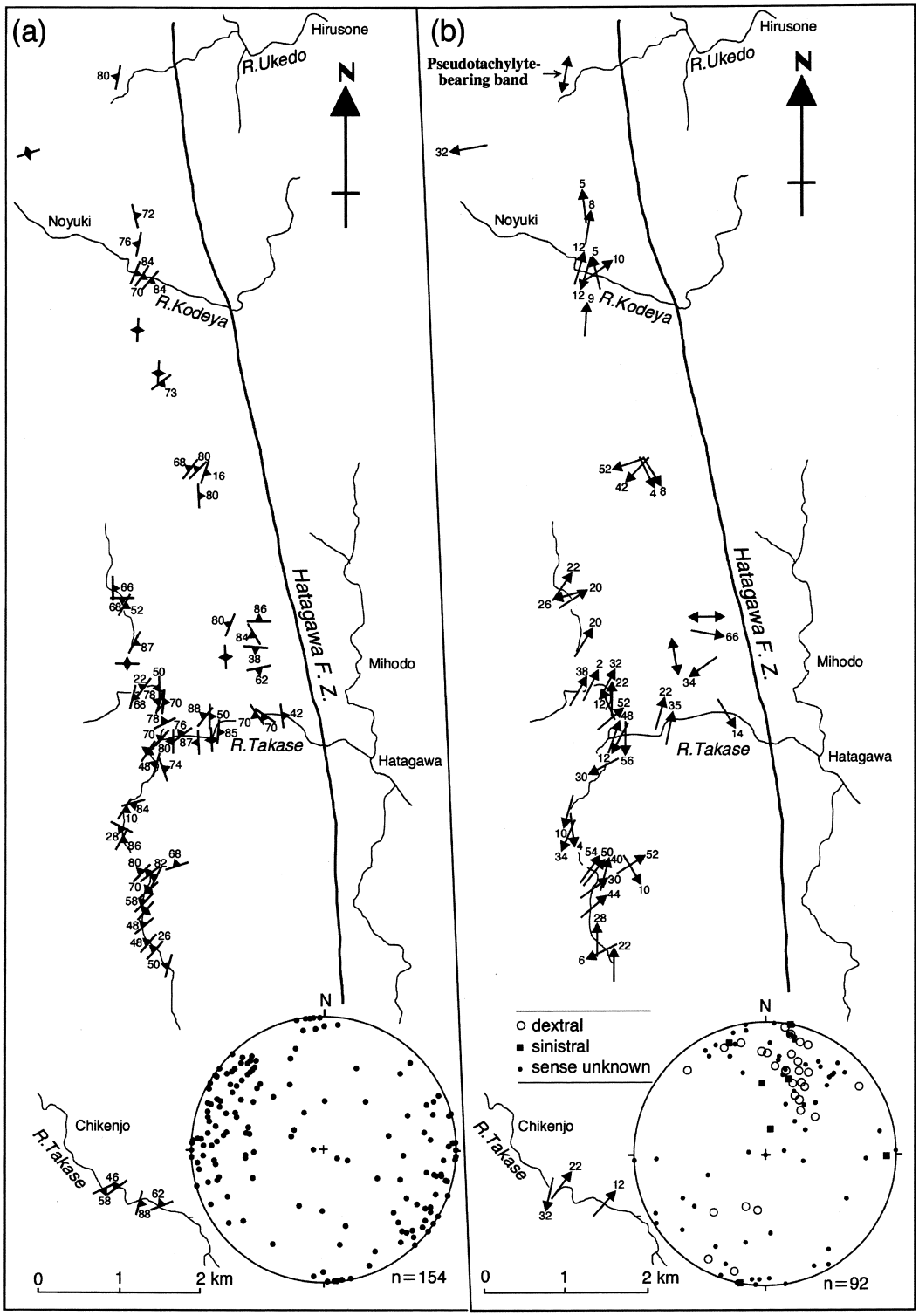

Fig. 2. Structural maps showing foliations (a) and lineations (b) of dark bands (mainly ultramylonite bands) and equal-area lower hemisphere projections. The symbols in the equal area projection of the lineation (b) denote the sense of shear.

T of ultramylonite bands and the displacement D (net slip) estimated by the separation of markers such as aplite veins and stretching lineations. The plots show that the D/T values vary from $10^{1.4}$ to $10^{2.2}$. These results are larger than those estimated from mylonites (10^0–10^1) but similar to those from fault gouges (10^1–10^3) or pseudotachylytes (10^1–10^2; Sibson, 1975; also see Nakamura and Nagahama, 1992).

The obliquity between foliation and band boundary, the step structure of the ridge-in-groove lineation and the asymmetric microstructures described in the next section indicate a predominant dextral shear for the NNE-trending shear zones, but a sinistral shear for E–W- or N–S-trending shear zones (Fig. 2b). From conjugate shear zones, σ_1 direction can be estimated as about ENE–WSW. Dextral shear on the NNE-trending dark bands (Fig. 2b) is unlikely to have formed in the same regional stress field as the sinistral shearing for the N–S-trending large shear zone on the east of the HFZ (Fig. 1).

4. Mineral composition and microstructures

Microscopic observation has been carried out on XZ thin sections cut normal to the foliation and parallel to the lineation. Well-foliated and laminated dark bands are commonly composed of ultramylonite. Some dark bands with foliation are also composed of foliated cataclasite, and it is sometimes difficult to distinguish ultramylonite and foliated cataclasite at the outcrop. Ultramylonite and cataclasite sometimes coexist in the same dark band. Matrix minerals in the dark bands are too small to observe under the microscope, and mineral species were identified from back-scattered electron image photographs using an electron probe microanalyzer (JEOL-JXA733).

4.1. Ultramylonite–fractured ultramylonite

Ultramylonite bands are dominantly composed of very fine-grained minerals, with opaque-rich thin seams (Fig. 6a, b). In some bands, rootless intrafolial flow folds are observed. The ultramylonite band has mesoscopically sharp planar margins. However, under the microscope they occasionally have embayments of fine-grained aggregate towards the surrounding granite or granitic mylonite. Such embayments often contact with biotite or hornblende grains within the surrounding granite (Fig. 6e).

Fine-grained matrix is mainly composed of quartz, plagioclase, K-feldspar, magnetite, mica and epidote (Fig. 6c, f). Fine-grained aggregates of feldspar surrounding a porphyroclast are sometimes stretched out into the matrix forming tails. The grain-size of matrix plagioclase and K-feldspar varies from submicrons to

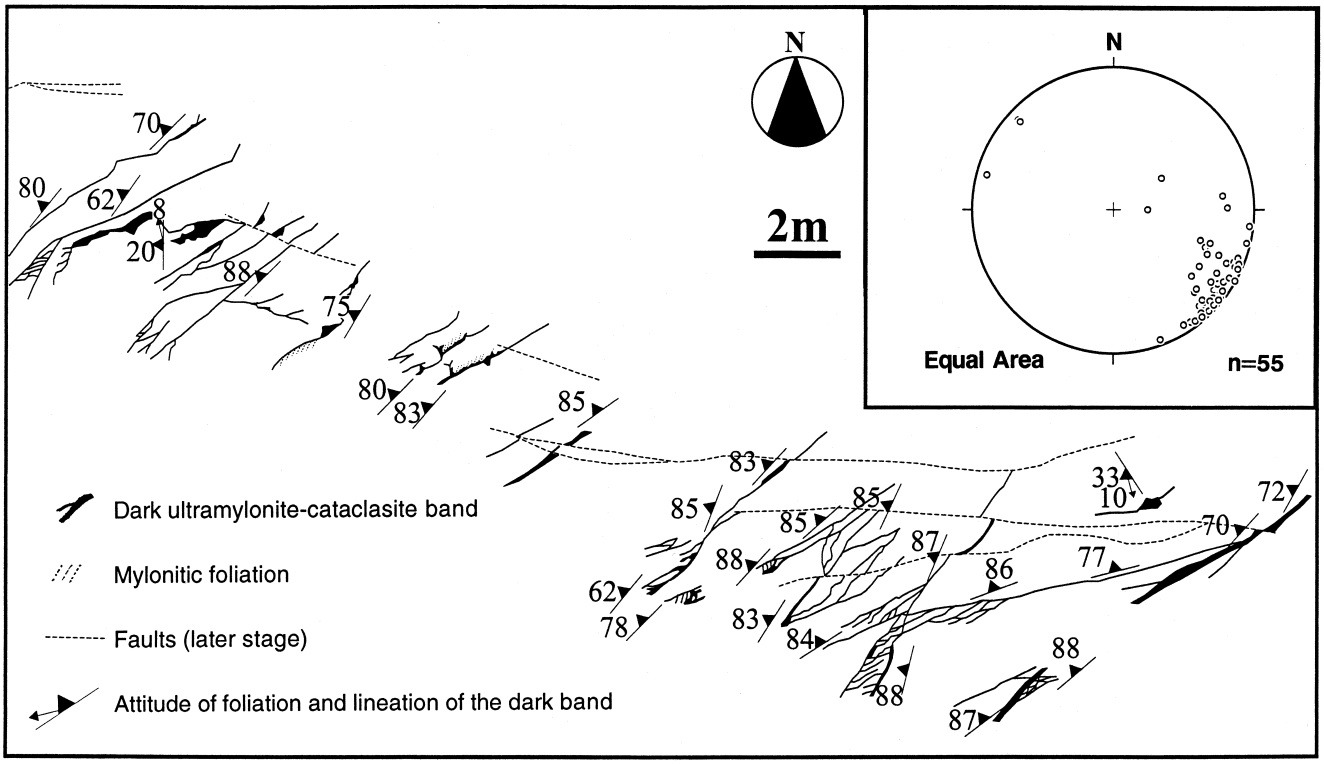

Fig. 3. Outcrop sketch showing the occurrence of ultramylonite and cataclasite bands at the location A (Fig. 1).

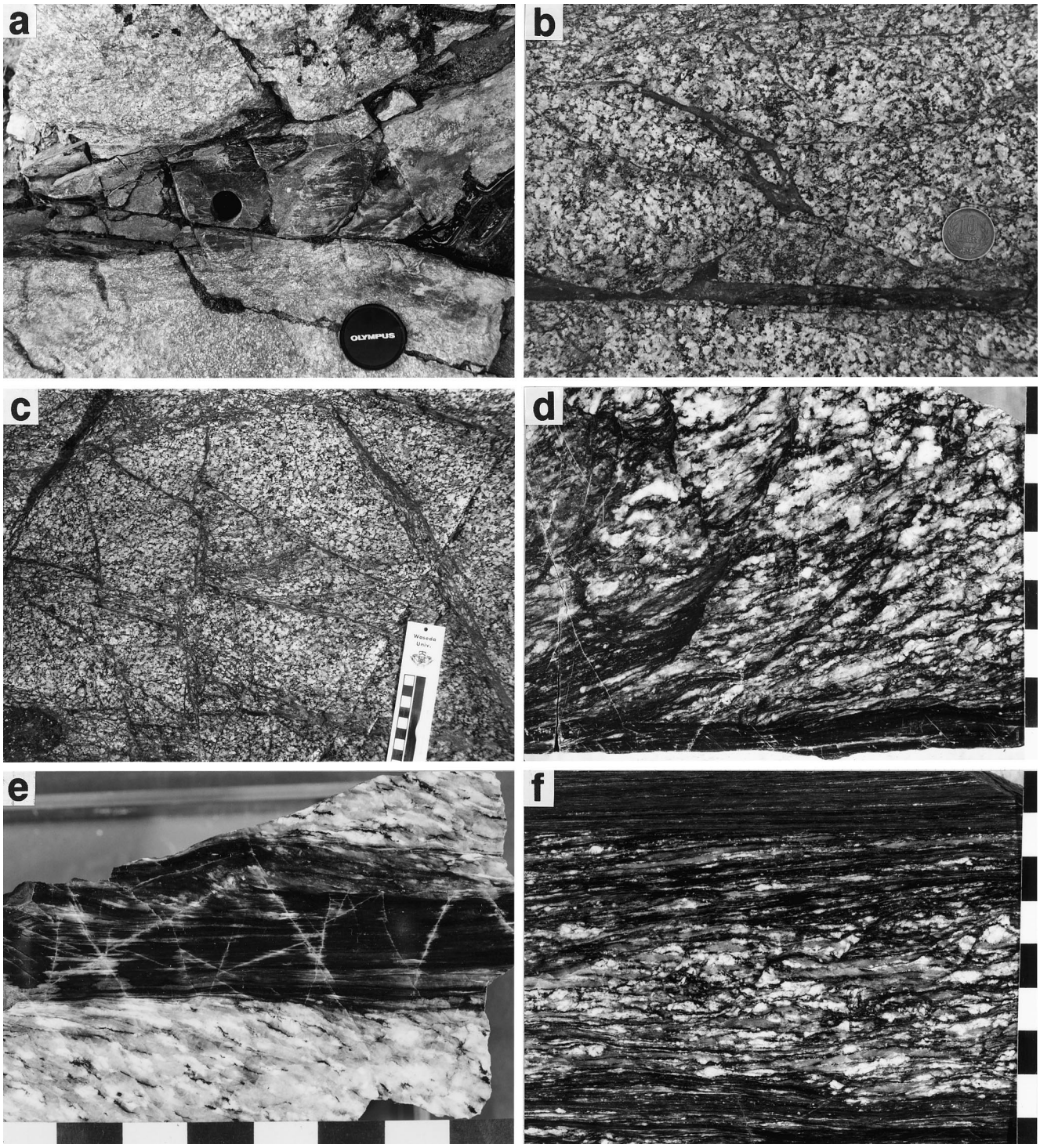

Fig. 4. Outcrops (a–c) and polished slices (d–f) showing the occurrence of dark bands along the Takase River. (a), (d), (e), (f) Ultramylonite–mylonite bands, (b), (c) cataclasite bands. (a) One of the thickest straight bands of ultramylonite at the location A (Fig. 1). The diameter of a lens cap is 6 cm. (b) Weakly foliated cataclasite band (bottom) from which the small dark bands branch off, 150 m west from location B (Fig. 1). (c) Cataclasite and foliated cataclasite bands (and possibly ultramylonite bands) forming a network at location B (Fig. 1). (d) Weakly mylonitized granitoid grades into the ultramylonite band (bottom) forming a sigmoidal foliation. Small ultramylonite bands branch off from the ultramylonite band at relatively high angles. (e) Typical ultramylonite band surrounded by weakly mylonitized granitoid showing curved foliation. (f) Paired ultramylonite bands intercalating mylonite. The foliation in the dark ultramylonite (a, d–f) is almost parallel to the band boundary reflecting a large value of shear strain. In each case (c–f), each scale of the black and white bar is 1 cm.

several microns. The existence of lattice preferred orientation (LPO) in the feldspar aggregates can be inferred under the microscope with the gypsum plate inserted. The LPO in the plagioclase aggregates in ultramylonite bands in the study area are determined using transmission electron microscopy (Shigematsu and Tanaka, 2000). Quartz aggregates commonly form lenticular lenses or asymmetric boudins (Fig. 6d, e), in which strong LPO can be observed with the gypsum plate inserted. Grain size of recrystallized quartz varies between several microns and tens of microns. The presence of these fine-grained (~30 μm) recrystallized quartz grains is common in ultramylonites (Takagi, 1998). Very fine-grained (1–3 μm) magnetite is commonly disseminated in the matrix of the dark bands with a modal percentage of about 2–3% as estimated by computer image analysis using electron backscattering. On the other hand, modal percentage of magnetite commonly associated with biotite in the surrounding granite is lower than 1%. Mica minerals (biotite or phengite) are fine grained and their content is generally lower in the ultramylonite than in the surrounding granitic protolith. This observation is also supported by the results of X-ray diffractometry of whole rocks (Fig. 7). In some samples, however, a larger amount of fine-grained biotite is present (Fig. 6d, g).

Porphyroclasts are commonly plagioclase and K-feldspar. Relatively large quartz grains in the matrix also constitute porphyroclasts or boudins (Fig. 6d). Porphyroclasts are commonly smaller than 100 μm, and the largest observed is ca. 700 μm. Their shape is commonly rounded, but some porphyroclasts in mica-rich samples show an irregular outline with embayments (Fig. 6g). Asymmetric pressure shadows composed of quartz and K-feldspar, and asymmetric tails composed of fine-grained aggregates of quartz, K-feldspar and plagioclase, envelop the porphyroclasts. Anastomosing aggregates of fine-grained recrystallized feldspars transect some feldspar porphyroclasts in the ultramylonites and surrounding mylonites (Fig. 6h). Grain size of this fine-grained aggregate varies from 0.2 μm to several microns on the basis of TEM observations (Shigematsu, 1999). Some ultramylonites were subsequently fractured to form cataclasite where the individual fragments preserve the ultramylonite foliation but are rotated with respect to each other (Fig. 8c).

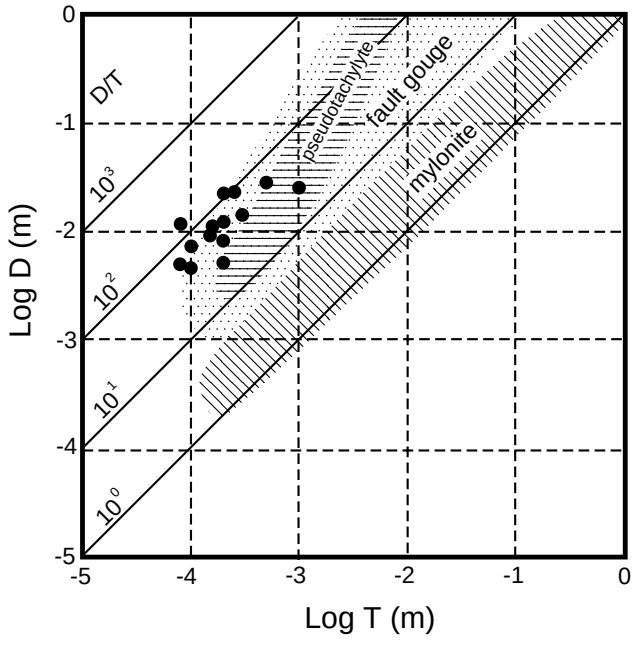

Fig. 5. Logarithmic plot of thickness (T) vs. displacement (net slip: D) in the investigated ultramylonite bands (dots). The outlined areas of mylonites, fault gouges, and pseudotachylytes are drawn after Nakamura and Nagahama (1992).

4.2. Cataclasite–mylonitized cataclasite

Many dark bands in the study area are composed of brecciated rock fragments or mineral clasts constituting dark or greenish gray, random-fabric or foliated cataclasites (Fig. 4b, c). The foliation in the cataclasites is defined by the alignment of elongate clasts. Cataclasite bands are composed of quartz, feldspar, epidote, mica, chlorite, and magnetite. They are often associated with epidote veins, and some cataclasites also contain large amounts of fine-grained epidote. Magnetite grains commonly larger than those in ultramylonite are also observed in cataclasite bands.

Localized ductile shear zones (about several hundred microns in thickness) are found in some cataclasites. In these shear zones, quartz fragments are strongly deformed and dynamically recrystallized (Fig. 8a, b). The grain size of recrystallized quartz varies from ten to several tens of micrometers. These mylonitized cataclasites also contain fine-grained epidote (Fig. 8d).

4.3. Pseudotachylyte–foliated pseudotachylyte

Pseudotachylyte has been reported from about 2 km north of Noyuki (Kubo and Takagi, 1997; Fig. 1). This dark and flinty pseudotachylyte vein (1–2 mm thick) is one of the paired veins (another vein is ultramylonite) interleaving a 5-cm-thick S–C mylonite (Fig. 9a). A thin cataclasite band is also present parallel to the pseudotachylyte vein (Fig. 9a). The pseudotachylyte vein is dark brown in color and has larger amounts of phyllosilicate minerals and lower magnetite content than the ultramylonite bands. The textural evidence for melting and quenching are: (1) injection veins branching off nearly perpendicular to the generation vein (Fig. 9b), (2) quartz fragments with irregular and rounded outlines some of which are surrounded by a cryptocrystalline aggregate, (3) con-

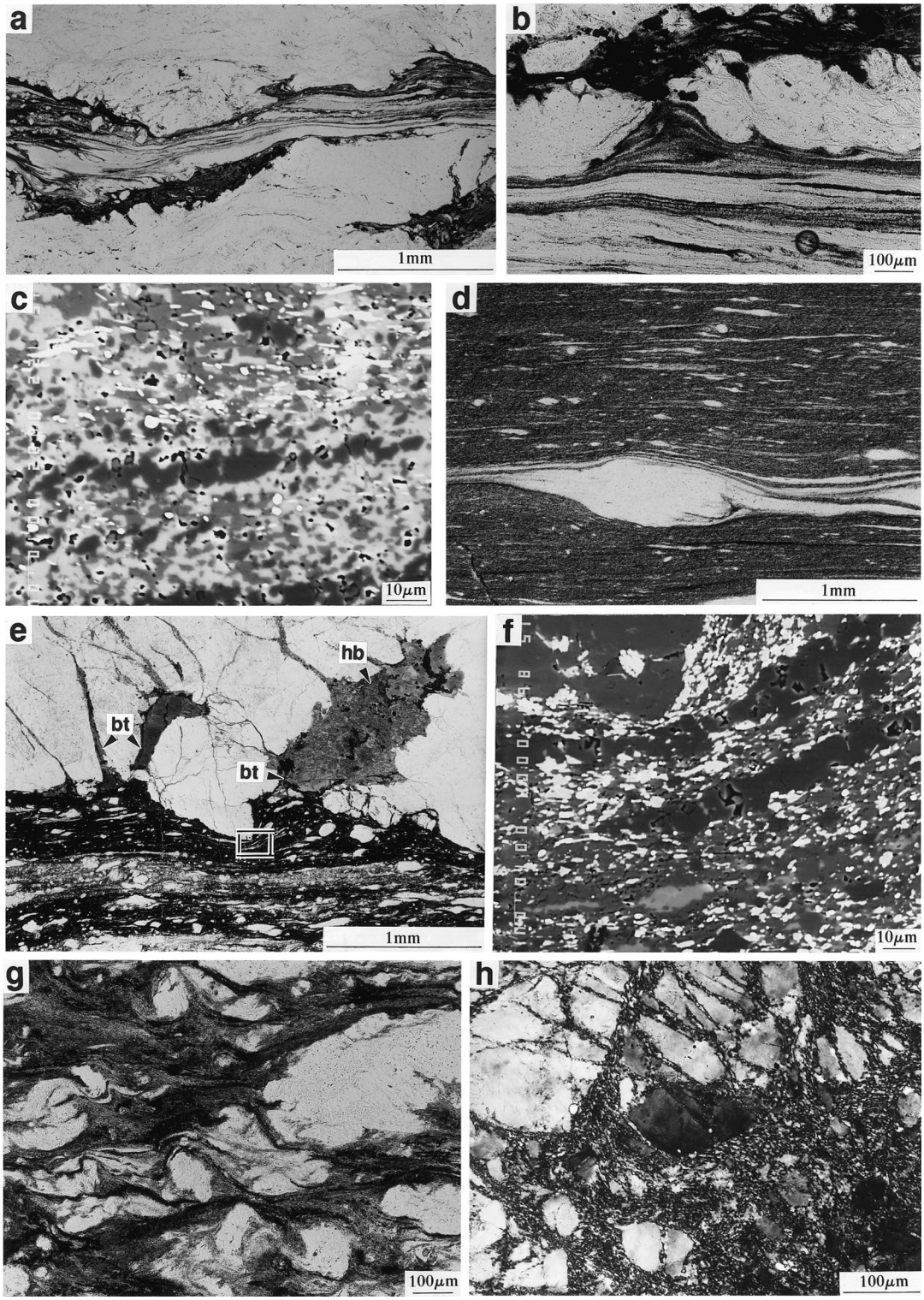

Fig. 6. Photomicrographs of ultramylonite bands. (a), (b) Well foliated ultramylonite bands with small-scale embayments possibly derived from the injection of pre-existing pseudotachylyte. (c) Fine-grained aggregate of K-feldspar (light), plagioclase (gray), quartz (dark), and minor biotite (white lath) and magnetite (white equont grain) in the matrix of ultramylonite. Grain size of constituent minerals is less than 10 μm. (d) Highly deformed lenticular quartz aggregate which is presumably derived from large fragment of cataclasite or of pseudotachylyte. (e) Embayment of ultramylonite at the contact with a biotite (bt) grain suggesting that this ultramylonite is possibly derived from pseudotachylyte, where selective melting has taken place. hb: hornblende. (f) Detail of the boxed area in (e) where quartz, plagioclase, K-feldspar, magnetite and epidote can be observed. (g) Ultramylonite consisting of quartzose fragments and a micaceous matrix. The outline of quartzose fragments is quite irregular with embayments suggesting pseudotachylyte origin. (h) Dynamically recrystallized K-feldspar forming very fine-grained aggregate, transecting the original K-feldspar porphyroclast. (a, b, d, e, g) Plane polarized light (PPL), (h) crossed polars (XPL), (c, f) back-scattered electron (BSE) image.

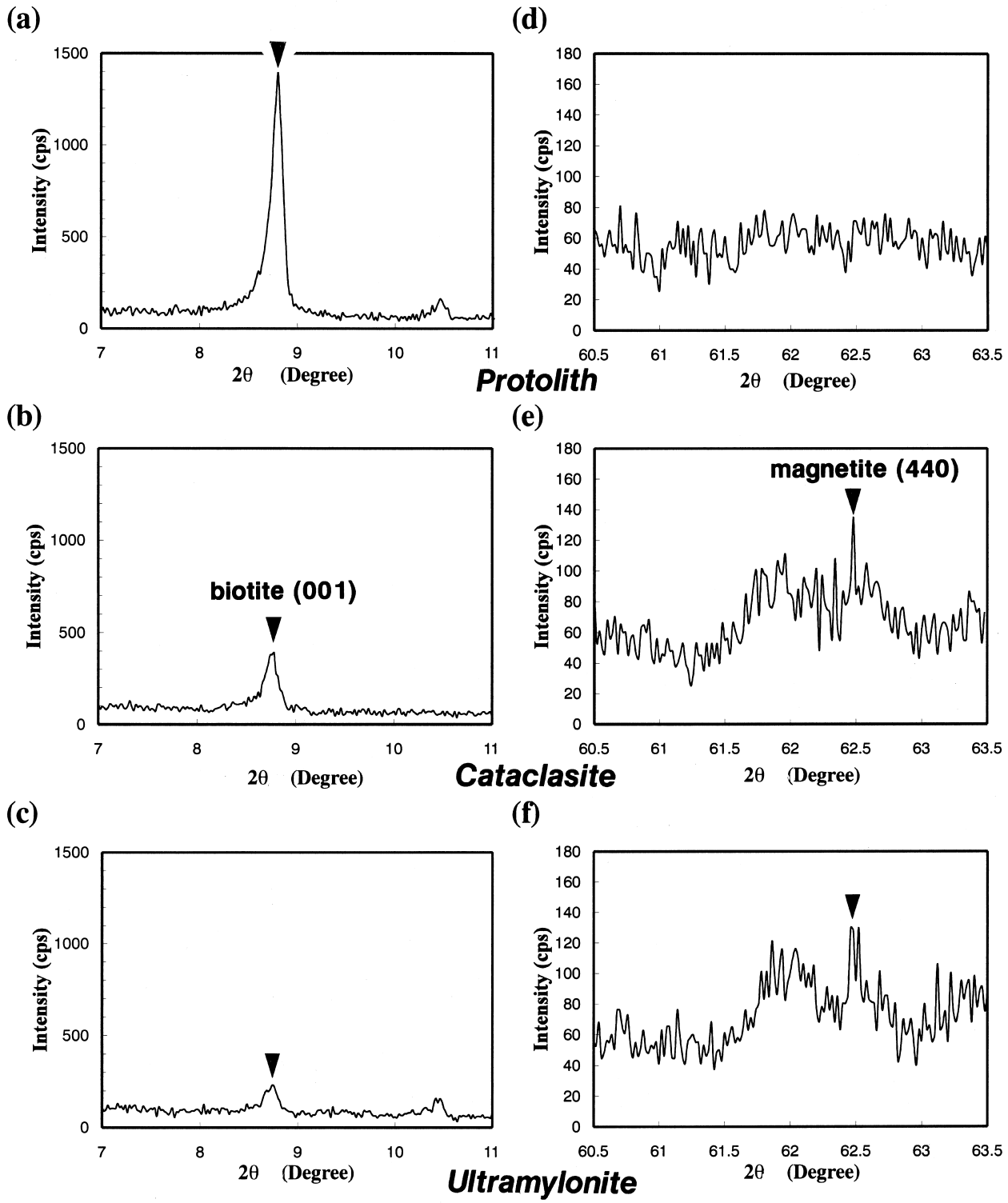

Fig. 7. X-ray diffraction patterns of biotite (a–c) and magnetite (d–f) from granitic protolith (a, d), cataclasite band (b, e) and ultramylonite band (c, f). Biotite contents decrease from protolith to cataclasite and ultramylonite as magnetite contents increase [cf. 10.1 Å peak (001) of biotite vs. 1.49 Å peak (440) of magnetite in each chart]. Magnetite contents in cataclasite and ultramylonite are also shown by BSE image photographs and magnetic susceptibility (see text).

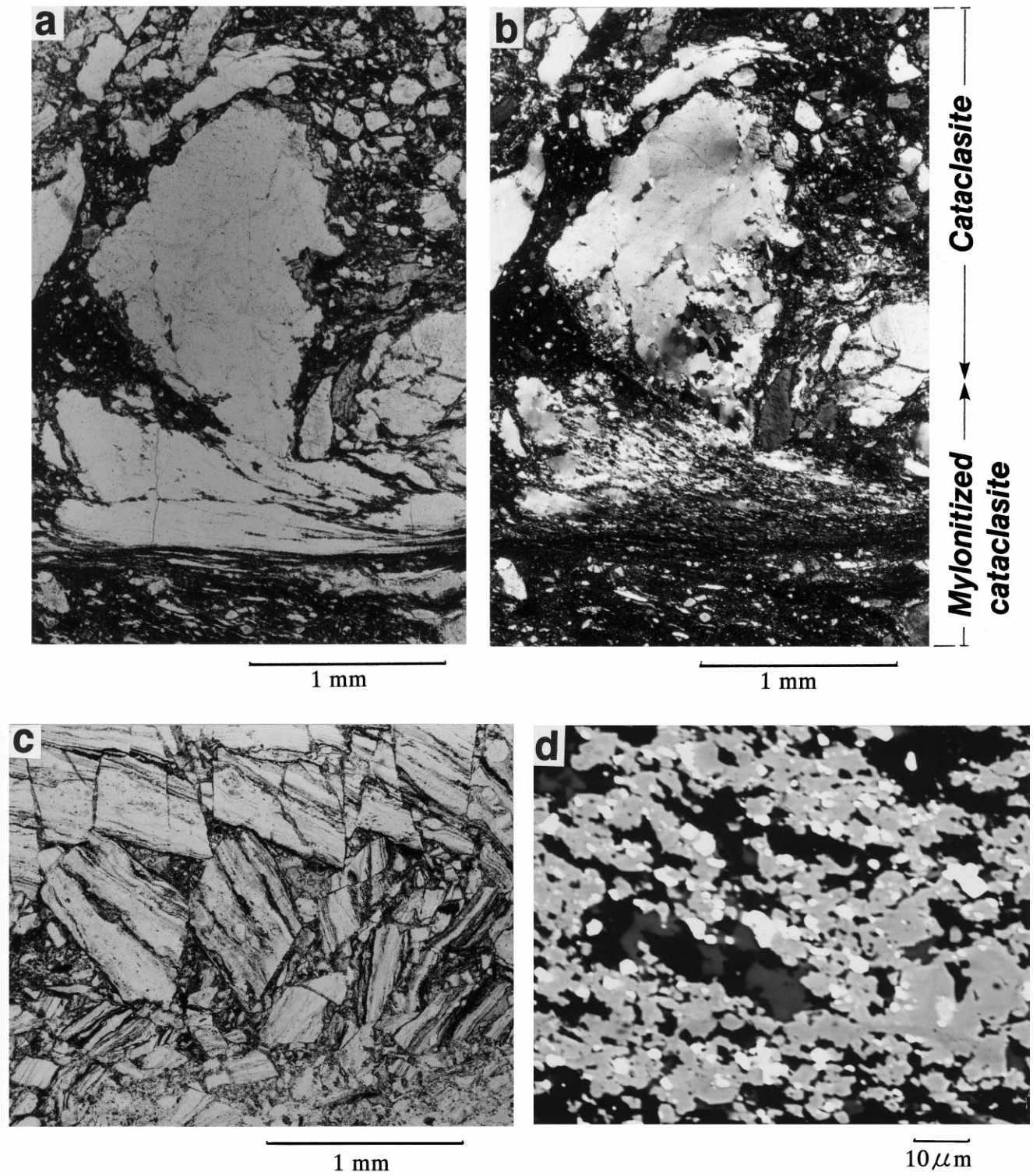

Fig. 8. Photomicrographs of mylonitized cataclasite (a, b, d), and cataclasis after the formation of ultramylonite (c). (a, b) Quartz fragments are stretched with dynamic recrystallization along the ductile shear zone where large amount of epidote grains together with recrystallized quartz and feldspar formed (d). (a, c) PPL, (b) XPL. (d) BSE image of the matrix domain of mylonitized cataclasite; white: opaque minerals, dull white: epidote, dark gray: K-feldspar, black: quartz and plagioclase.

centric texture, a kind of spherulite (e.g. Lin, 1994), with small cores composed of quartz or feldspar fragments (Fig. 9c; Kubo and Takagi, 1997).

In the generation veins, both quartz fragments and concentric textures are deformed and define an *S* surface. Asymmetric pressure shadows (Fig. 9d), mainly composed of K-feldspar, can be observed forming wings on quartz fragments in the generation vein. In contrast, no visible deformation of fragments was observed in the injection vein (Fig. 9b).

5. Magnetic susceptibility

Granitic rocks in the Abukuma Belt on the west of the HFZ belong dominantly to the ilmenite series, with

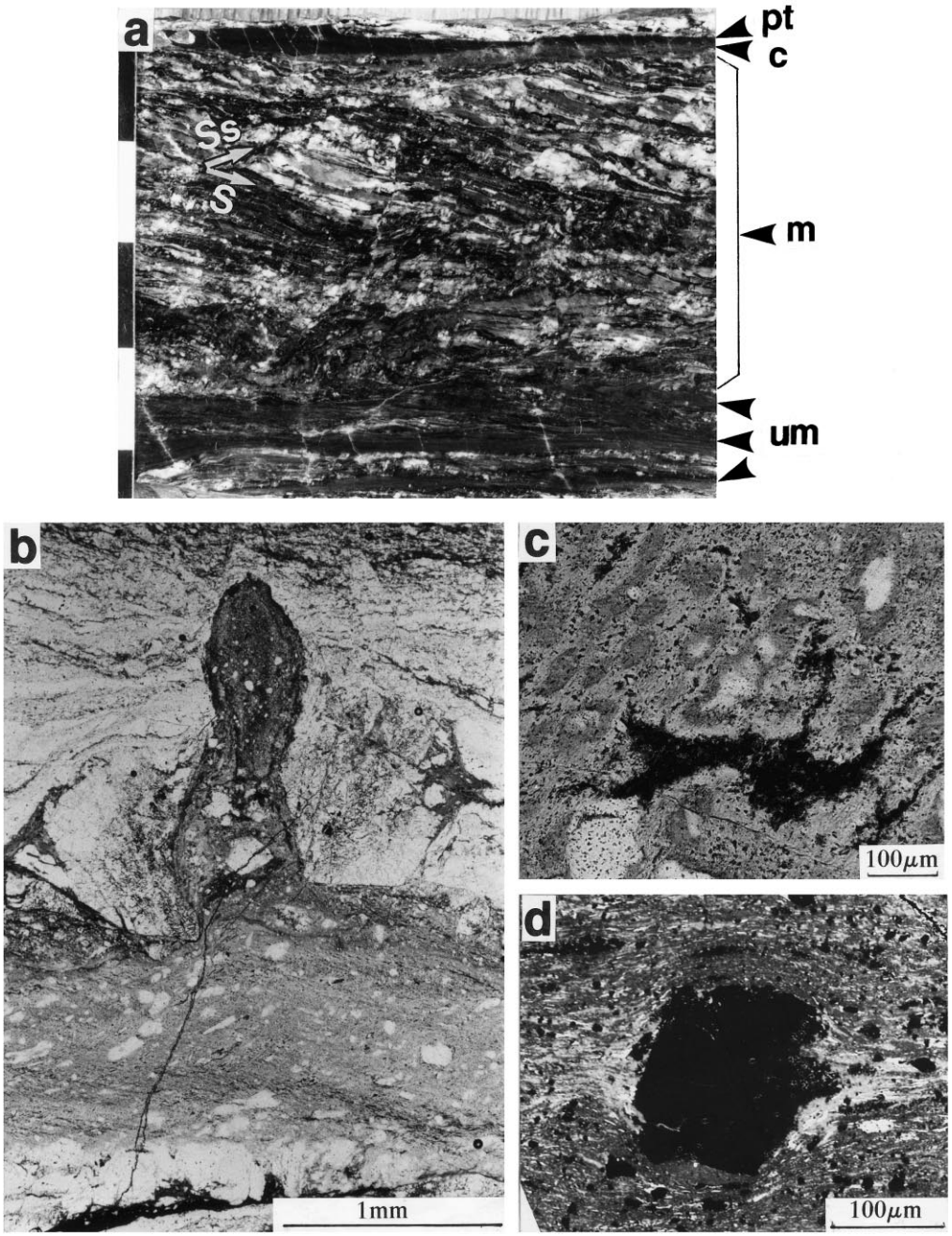

Fig. 9. Sheared pseudotachylyte found by Kubo and Takagi (1997). (a) Occurrence of pseudotachylyte vein (pt) associated with cataclasite (c), *S–C* mylonite (m) and ultra-mylonite (um). Ss: shear bands. (b) Photomicrograph of sheared pseudotachylyte with injection vein. Note that the fragments in the injection vein are not plastically deformed whereas those in the generation vein are deformed. PPL. (c) Weakly deformed spherulite in the matrix of pseudotachylyte. PPL. (d) BSE image of pressure shadow which consists dominantly of K-feldspar adjacent to a quartz fragment in the generation vein.

a low magnetic susceptibility (Kanaya and Ishihara, 1973; Kubo and Yamamoto, 1990), and magnetite grains are rarely observed under the reflected light microscope. However, in the study area, magnetite grains do exist not only in the ultramylonite bands but also in the cataclasite bands and surrounding granitic rocks. We have measured the volume magnetic susceptibility (MS) using a magnetometer (Kappameter KT-5) at flat and fresh outcrops. The boundary value in the magnetic susceptibility between magnetite series and ilmenite series is about 3.4×10^{-3} (SI unit) for granitic rocks (e.g. Sato and Ishihara, 1983). The MS determined for thick, dark ultramylonite bands has a range of $20–34 \times 10^{-3}$ SI (unit) and the MS for granitic rocks with fractures surrounding the ultramylonite bands varies between one and 12. In contrast, the undeformed fresh granites without any observable dark bands and/or fractures commonly show MS values lower than 2. This high magnetic susceptibility in the ultramylonite bands is attributed to the existence of very fine-grained magnetite, as described earlier.

6. Chemical composition

The bulk chemical composition of the dark bands and surrounding undeformed granitic rocks was analyzed using XRF (Rigaku, system 3070) through the glass-bead method. The sample preparation and analytical conditions are outlined in Uchida et al. (1987). The XRF analyses were carried out in two samples of the pink biotite granite (G1,2) and associated ultramylonite bands (B1,2), and five samples of the hornblende-bearing biotite granodiorite (G3–8) and associated ultramylonite bands (U3–8) and cataclasite bands (C7,8).

The results of XRF analyses are shown in Table 1. The major element content in the all ultramylonite bands and one cataclasite band (C8) is very similar to those in the surrounding granitic rocks as shown in the isocon diagram (Grant, 1986) in Fig. 10. These results indicate that the ultramylonite and some cataclasite bands are formed through in-situ deformation of the granitic protolith without significant mass transfer in or out these shear zones. On the other hand, the contents of some major elements such as Ca, Fe and Mg in the cataclasite band C7 is quite different from those of the surrounding granitic rock G7. This difference for C7 is probably due to the large amount of epidote formed by hydrothermal alteration in this band (Fig. 7h).

7. Discussion

Cataclastic and plastic deformation features closely

Table 1
XRF analytical results showing the major element content of ultramylonite (U1–U8), cataclasite (C7, C8) and granitic protoliths (G1–G8)

Granitic protolith									
	Biotite granite		Hornblende-bearing biotite granodiorite						
	G1	G2	G3	G4	G5	G6	G7	G8	
SiO_2	76.17	76.29	68.25	70.88	69.99	70.82	74.07	70.32	
TiO_2	0.05	0.05	0.36	0.32	0.35	0.33	0.23	0.31	
$Al2O_3$	12.35	12.92	15.25	14.42	15.10	14.37	13.15	15.65	
Fe_2O_3	0.97	1.03	3.60	3.15	3.24	3.33	2.04	2.78	
MnO	0.02	0.03	0.07	0.07	0.07	0.07	0.03	0.05	
MgO	0.05	0.03	0.62	0.56	0.61	0.65	0.31	0.48	
CaO	0.81	0.89	2.55	2.36	2.63	2.37	1.23	2.51	
Na_2O	2.42	3.26	3.41	3.21	3.61	3.08	3.40	3.98	
K_2O	4.92	4.73	3.48	3.19	3.39	3.36	3.78	4.04	
P_2O_5	0.01	0.01	0.08	0.07	0.07	0.08	0.04	0.09	
Total	97.77	99.24	97.67	98.23	99.06	98.46	98.28	100.21	
Ultramylonite band								Cataclasite band	
	U1	U2	U3	U4	U5	U6	U8	C7	C8
SiO_2	74.38	77.31	69.48	70.41	71.16	71.92	65.97	70.41	69.12
TiO_2	0.06	0.05	0.35	0.32	0.34	0.31	0.42	0.40	0.33
Al_2O_3	12.81	12.81	14.67	14.38	14.52	13.48	16.90	14.04	16.08
Fe_2O_3	1.85	1.18	3.45	3.19	3.11	3.31	3.69	3.87	2.63
MnO	0.04	0.02	0.07	0.07	0.07	0.06	0.06	0.09	0.03
MgO	0.13	0.03	0.63	0.55	0.58	0.61	0.67	0.75	0.47
CaO	1.15	0.95	2.80	2.43	2.75	2.19	3.02	2.92	2.64
Na_2O	3.22	3.18	3.14	3.04	4.50	3.70	5.93	3.23	4.97
K_2O	4.11	4.50	3.40	3.65	2.12	2.68	2.73	2.30	3.11
P_2O_5	0.01	0.01	0.08	0.07	0.08	0.07	0.11	0.10	0.09
Total	97.76	100.04	98.07	98.11	99.23	98.33	99.50	98.11	99.47

coexist in the dark bands on the west of the HFZ described in this paper. This observation can be explained by the following two different generation paths: (1) the deformation environment has switched from dominantly plastic to dominantly cataclastic, or vice versa, (2) co-seismic fracturing and interseismic plastic flow alternated in the cataclastic–plastic transition zone. If the former occurred, all the ultramylonite and mylonite bands are expected to be overprinted by cataclasis or crosscut by cataclasite and pseudotachylyte bands, or vice versa. If both shear zones formed by the latter mechanism, a cyclic generation of the cataclasite (+pseudotachylyte) and ultramylonite is inferred to have occurred, and variable overprinting relationships between cataclasis and plastic deformation are expected.

In some samples, the rotated fragments in the cataclasite bands are, themselves, ultramylonite with fine-grained recrystallized quartz with a strong foliation (Fig. 8c). This clearly indicates that some ultramylonites have been subjected to subsequent cataclasis. On the other hand, fragments of cataclasite can be observed along the thinly embedded mylonite zone in cataclasite and exhibit dynamically recrystallized quartz indicating overprinting plastic deformation (Fig. 8a, b). This clearly indicates that the cataclasite was partly mylonitized to form the ultramylonite layer. Such mylonitized cataclasites are also described in Simpson (1986) and Guermani and Pennacchioni (1998).

The presence of secondary epidote and magnetite in the cataclasite and ultramylonite bands suggests fluid activity in these domains. Thus, hydrolytic weakening and reaction softening promoted by infiltration of hydrothermal fluid along fractures are also possible (e.g. Segall and Pollard, 1983; White and White, 1983; Segall and Simpson, 1986; Simpson, 1986; Gibson, 1990; Tourigny and Tremblay, 1997).

In the ultramylonite bands, the grain size of the feldspar aggregate is very fine (Fig. 6h), and a lattice preferred orientation can be observed (Shigematsu and Tanaka, 2000). These features suggest the operation of crystal–plastic processes in feldspar (Tullis and Yund, 1985). TEM observations (Shigematsu, 1999; Shigematsu and Tanaka, 2000) also confirm that crystal–plastic processes have operated in ultramylonite bands on the west of the HFZ. If cataclastically deformed materials underwent crystal–plastic deformation, a narrow ultramylonite band would be developed (Tullis et al., 1990). This interpretation is also supported by the evidence that the D/T values of the ultramylonite bands are similar to those determined in fault gouge and pseudotachylyte (Fig. 5). These high D/T values reflect a strong shear localization as also demonstrated by the very low S–C angles ($<1^{\circ}$). The occurrence of strain localization at both margins of the weakly deformed granite, constituting paired bands (e.g. Figs. 4f and 9a), also suggests the existence of brittle precursors for plastic deformation (Grocott, 1981; Tourigny and Tremblay, 1997).

In the pseudotachylyte, the presence of ductilely deformed and oriented fragments in the generation vein and of undeformed fragments in the injection vein (Kubo and Takagi, 1997) suggest that mylonitic deformation occurred after consolidation of the pseudotachylyte (Fig. 9). Although there is little direct evidence of primary fusion in the ultramylonite bands because of the strong deformation and complete recrystallization of quartz and feldspar, the following features in some ultramylonite bands are

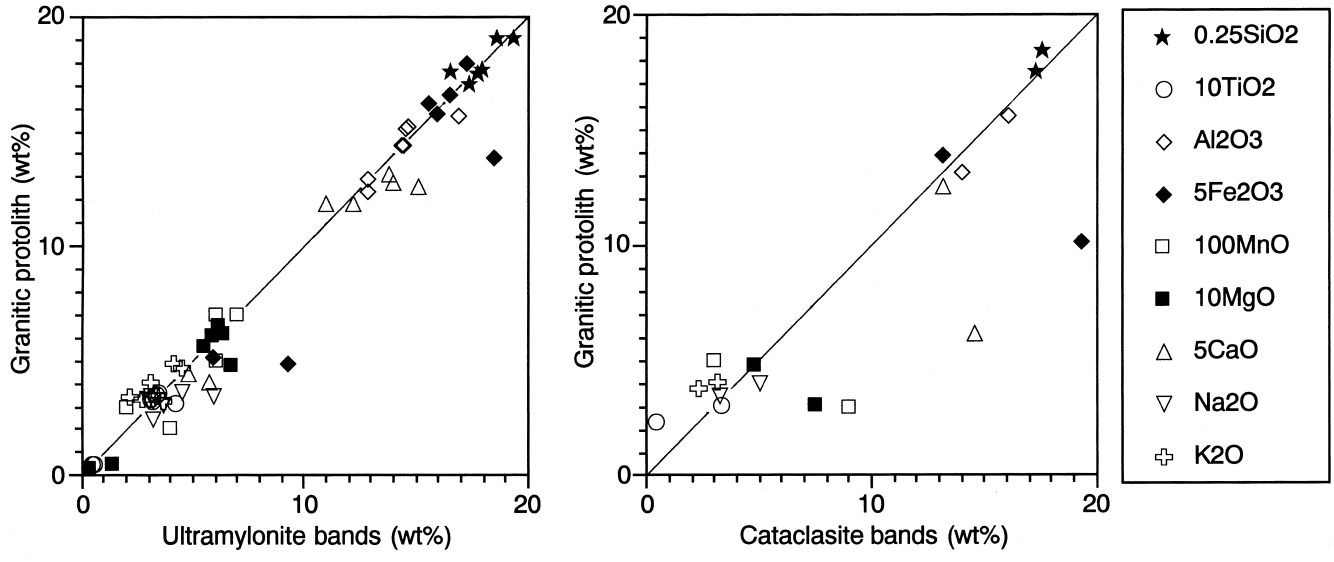

Fig. 10. Isocon diagrams showing the major element content of ultramylonite and cataclasite bands with respect to the granitic protolith.

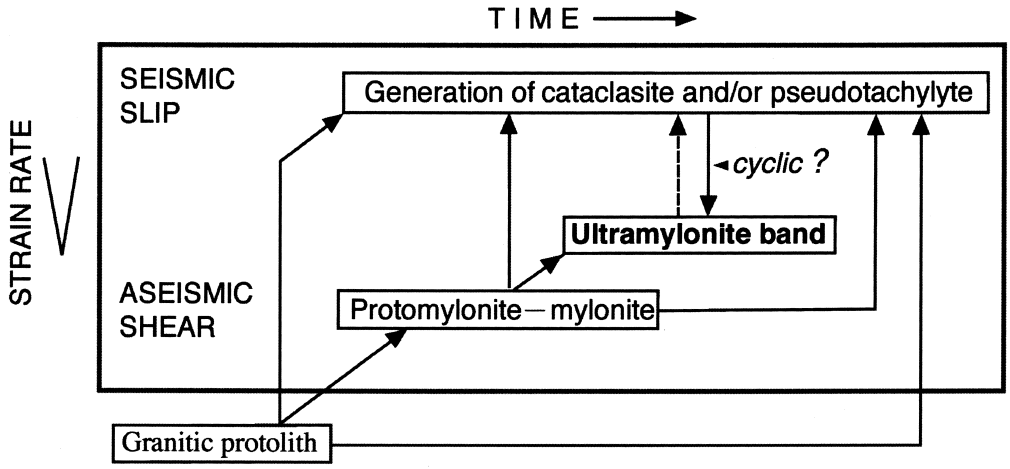

Fig. 11. Schematic diagram showing the cyclic generation of plastic and cataclastic fault rocks in the cataclastic–plastic transition zone of the granitic crust.

similar to those of pseudotachylyte: (1) the presence of convex embayments from fine-grained matrix into biotite or hornblende grains of the granitic protolith (see Passchier and Trouw, 1996, p. 101), (2) the existence of very fine-grained magnetite in the matrix (see Phillpotts, 1964), (3) the irregular outline with embayments of some porphyroclasts, and (4) the similar bulk chemical composition with the granitic protolith. The coexistence of these features in some ultramylonite bands strongly suggests the possibility of plastic deformation occurring after formation of pseudotachylyte.

In summary, some cataclastically deformed bands are inferred to have changed into plastically deformed ultramylonite by the mechanisms mentioned above. Accordingly, the small-scale shear zones on the west of the HFZ are inferred to have been formed at the cataclastic–plastic transition zone (ca. 10–15-km-deep, greenschist facies conditions), where co-seismic fracturing and aseismic plastic deformation have probably taken place repeatedly (Fig. 11). Thus, the focal area of the intracontinental large earthquakes in the cataclastic–plastic transition zone may consist of a network of bands of fine-grained cataclastic and plastic fault rocks as described here, and the rheology of these fault rocks must play an important role for earthquake generation.

Acknowledgements

We express sincere thanks to Drs. H. Nagahama (Tohoku University) and K. Kubo (GSJ) for giving us valuable information and comments. Thanks are also due to Dr. S. Omori, Mrs. S. Kinouchi and K. Yonemochi for supporting EPMA and XRF analyses, and to Mr. K. Saga for preparation of thin sections in Waseda University. Thanks are also due to Dr. J. Hippertt who gave us constructive comments and improved our English. This research was partly supported by the Annual Project organized by Waseda University (No. 94A-211).

References

Ando, M., 1995. Foreshocks, main shock, after shocks and induced earthquakes of the 1995 Southern Hyogo Earthquake. Chikyu (Earth Monthly) Special No. 13, 18–29.

Brace, W.F., Kohlstedt, D.L., 1980. Limits on lithospheric stress imposed by laboratory experiments. Journal of Geophysical Research 85, 6248–6252.

Byerlee, J.D., 1978. Friction of rocks. Pure and Applied Geophysics 116, 615–626.

Das, S., Scholz, C.H., 1983. Why large earthquakes do not nucleate at shallow depths. Nature 305, 621–623.

Gibson, R.G., 1990. Nucleation and growth of retrograde shear zones: an example from the Needle Mountains, Colorado, U.S.A. Journal of Structural Geology 12, 339–350.

Goto, K., Takeuchi, S., Takagi, H., 1994. Dark ultramylonite bands to the west of Hatagawa Fracture Zone in the Namie area, Fukushima Prefecture, Northeast Japan—occurrence and chemical composition. Abstracts of the 101st Annual Meeting of the Geological Society of Japan, 268 (in Japanese).

Grant, J.A., 1986. The isocon diagram — a simple solution to Gresens' equation for metasomatic alteration. Economic Geology 81, 1976–1982.

Grocott, J., 1981. Fracture geometry of pseudotachylyte generation zones: a study of shear fractures formed during seismic events. Journal of Structural Geology 3, 169–178.

Guermani, A., Pennacchioni, G., 1998. Brittle precursors of plastic deformation in a granite: an example from the Mont Blanc massif (Helvetic, western Alps). Journal of Structural Geology 20, 135–148.

Hobbs, B.E., Means, W.D., Williams, P.E., 1976. An Outline of Structural Geology. John Wiley & Sons, New York.

Hobbs, B.E., Ord, A., Teyssier, C., 1986. Earthquakes in the ductile regime? Pure and Applied Geophysics 124, 309–336.

Kanaya, H., Ishihara, S., 1973. Regional variation of magnetic susceptibility of the granitic rocks in Japan (in Japanese with English abstract). Journal of Mineralogy, Petrology and Economic Geology 68, 211–224.

Kirby, S.H., 1980. Tectonic stresses in the lithosphere: Constraints provided by the experimental deformation of rocks. Journal of Geophysical Research 85, 6353–6363.

Koch, N., Masch, L., 1992. Formation of Alpine mylonites and pseudotachylytes at the base of the Silvretta nappe, Eastern Alps. Tectonophysics 204, 289–306.

Koshiya, S., 1988. Quartz c-axis fabric and microstructures in mylonite—An application to the Hatakawa Shear Zone, northeast Japan (in Japanese with English abstract). Journal of the Tectonic Research Group of Japan 33, 13–32.

Kubo, K., Takagi, H., 1997. New finding of pseudotachylyte from the Abukuma Granites on the west of Hatagawa Fracture Zone (in Japanese with English abstract). Journal of the Geological Society of Japan 103, 798–801.

Kubo, K., Yamamoto, T., 1990. Cretaceous intrusive rocks of the Haramachi district, eastern margin of the Abukuma mountains—petrography and K–Ar age (in Japanese with English abstract). Journal of the Geological Society of Japan 96, 731–743.

Kubo, K., Yanagisawa, Y., Yoshioka, T., Takahashi, Y., 1994. Geology of the Namie and Iwaki-Tomioka District. With Geological Sheet Map at 1:50,000, Geological Survey of Japan, 104 pp (in Japanese with English abstract).

Kubo, K., Yanagisawa, Y., Yoshioka, T., Yamamoto, T., Takizawa, F., 1990. Geology of the Haramachi and Omika District. With Geological Sheet Map at 1:50,000, Geological Survey of Japan, 155 pp (in Japanese with English abstract).

Lin, A., 1994. Microlite morphology and chemistry in pseudotachylite, from the Fuyun Fault Zone, China. Journal of Geology 102, 317–329.

Nakamura, N., Nagahama, H., 1992. Thickness and displacement of shear zones. Abstracts of the 99th Annual Meeting of the Geological Society of Japan, 364 (in Japanese).

Otsuki, K., Ehiro, M., 1992. Cretaceous left-lateral faulting in Northeast Japan and its bearing on the origin of geologic structure of Japan (in Japanese with English abstract). Journal of Geological Society of Japan 98, 1097–1112.

Passchier, C.W., 1982. Pseudotachylyte and the development of ultramylonite bands in the Saint-Barthelemy Massif, French Pyrenees. Journal of the Structural Geology 4, 69–79.

Passchier, C.W., 1984. The generation of ductile and brittle shear bands in a low-angle mylonite zone. Journal of Structural Geology 6, 273–281.

Passchier, C.W., Trouw, R.A.J., 1996. Microtectonics. Springer-Verlag, Berlin.

Phillpotts, A.R., 1964. Origin of pseudotachylites. American Journal of Science 262, 1008–1035.

Sato, K., Ishihara, S., 1983. Chemical composition and magnetic susceptibility of the Kofu granitic complex. Bulletin of the Geological Survey of Japan 34, 413–427.

Scholz, C.H., 1988. The brittle/plastic transition and the depth of seismic faulting. Geologische Rundschau 77, 319–328.

Scholz, C.H., 1990. The Mechanics of Earthquakes and Faulting. Cambridge University Press, Cambridge, UK.

Segall, P., Pollard, D.D., 1983. Nucleation and growth of strike-slip faults in granite. Journal of Geophysical Research 88, 555–568.

Segall, P., Simpson, C., 1986. Nucleation of ductile shear zones on dilatant fractures. Geology 14, 56–59.

Shigematsu, N., 1994. Grain-shape modification during dynamic recrystallization of quartz and deformation environment of the crust (in Japanese). Chikyu (The Earth monthly) 16, 754–759.

Shigematsu, N., 1999. Dynamic recrystallization in deformed plagioclase during progressive shear deformation. Tectonophysics 305, 437–452.

Shigematsu, N., Goto, K., 1995. The internal structures of shear zones estimated to be formed at the brittle ductile transition (in Japanese). Abstracts of the 102nd Annual Meeting of the Geological Society of Japan 485, 340.

Shigematsu, N., Tanaka, H., 2000. Dislocation creep of fine-grained recrystallized plagioclase under low temperature conditions. Journal of Structural Geology 22, 65–79.

Sibson, R.H., 1975. Generation of pseudotachylyte by ancient seismic faulting. Geophysical Journal of the Royal Astronomical Society 43, 775–794.

Sibson, R.H., 1977. Fault rocks and fault mechanisms. Journal of the Geological Society of London 133, 191–213.

Sibson, R.H., 1980. Transient discontinuities in ductile shear zones. Journal of Structural Geology 2, 165–174.

Sibson, R.H., 1982. Fault zone models, heat flow, and the depth distribution of earthquakes in the continental crust of the United States. Bulletin of the Seismological Society of America 72, 151–163.

Sibson, R.H., 1983. Continental fault structure and the shallow earthquake source. Journal of the Geological Society of London 140, 741–767.

Simpson, C., 1986. Fabric development in brittle-to-ductile shear zones. Pure and Applied Geophysics 124, 269–287.

Takagi, H., 1998. Fault rocks in the cataclastic–plastic transition zone. Memoirs of the Geological Society of Japan, No. 50, 59–72 (in Japanese with English abstract).

Tourigny, G., Tremblay, A., 1997. Origin and incremental evolution of brittle/ductile shear zones in granitic rocks: natural examples from the southern Abitibi Belt, Canada. Journal of Structural Geology 19, 15–27.

Tullis, J., Dell'Angelo, L., Yund, R.A., 1990. Ductile shear zone from brittle precursors in feldspathic rocks: the role of dynamic recrystallization. In: Duba, A.G., Durham, W.B., Handin, J.W., Wang, H.F. (Eds.), The brittle and ductile transition in rocks, Geophysical Monograph, 56. American Geophysical Union, Washington DC, pp. 67–82.

Tullis, J., Yund, R.A., 1985. Dynamic recrystallization of feldspar: a mechanism for ductile shear zone formation. Geology 10, 227–230.

U.S. Geological Survey Staff, 1990. The Loma Prieta, California, earthquake: An anticipated event. Science 247, 286-293.

Uchida, E., Takano, M., Nakamura, T., Imai, N., 1987. X-ray fluorescence analysis of silicate rocks (1) Analysis of major components (in Japanese with English abstract). Bulletin of Science and Engineering Research Laboratory, Waseda University 117, 35–41.

White, J.C., 1996. Transient discontinuities revisited: pseudotachylyte, plastic instability and the influence of low pore fluid pressure on deformation processes in the mid-crust. Journal of Structural Geology 18, 1471–1486.

White, J.C., White, S.H., 1983. Semi-brittle deformation within the Alpine fault zone, New Zealand. Journal of Structural Geology 5, 579–589.